BULLETIN OF THE POLISH ACADEMY OF SCIENCES
TECHNICAL SCIENCES
DOI: 10.24425/bpasts.2024.151959



# Mechanical energy absorption capacity of the porous Ti-6Al-4V alloy under quasi-static and dynamic compression

**Pavlo E. Markovsky[1], Jacek Janiszewski[2], Oleksandr O. Stasiuk[1], Dmytro G. Savvakin[1], Denys V. Oryshych[1], Piotr Dziewit[2]**

[1] G.V. Kurdyumov Institute for Metal Physics of NAS of Ukraine, 36, Vernadsky Blvd., 03142, Kyiv, Ukraine
[2] Military University of Technology, 2, gen. Sylwester Kaliski str., 00 – 908 Warsaw 46, Poland

**Abstract.** Porous materials are very efficient in absorbing mechanical energy in different applications. In the present study, porous materials based on the Ti-6(wt.%)Al-4V alloy were manufactured with the use of two different powder metallurgy methods: i) blended elemental powder approach using titanium hydride (TiH2) as well as V-Al master alloy powders and ii) using hydrogenated Ti-6-4 pre-alloyed powder. The powder compacts were sintered with additions of ammonium bicarbonate as a pore-holding removable agent. The emission of hydrogen from hydrogenated powders on vacuum sintering and the resulting shrinkage of powder particles permitted the control of the sintering process and creation of anticipated porous structures. Mechanical characteristics were evaluated under quasi-static and dynamic compressive loading conditions. Dynamic compression tests were performed using the direct impact Hopkinson pressure bar technique. All investigations aimed at characterizing the mechanical energy-absorbing ability of the obtained porous structures. The anticipated strength, plasticity, and energy-absorbing characteristics of porous Ti-6-4 material were evaluated, and the possibilities of their application were also discussed. Based on the obtained results, it was found that porous Ti-6-4 material produced with a blended elemental powder approach showed more promising energy absorption properties in comparison with pre-alloyed powder.

**Key words:** porous titanium and alloys, mechanical properties, high strain rate testing, direct impact Hopkinson pressure bar technique, microstructure influence, deformation mechanism, energy absorption

## 1. INTRODUCTION

Metallic materials with controlled porosity are characterized by several unique physical and mechanical properties, due to which they are widely used in various fields - from filters to impact energy-absorbing systems [1–4]. A wide range of different technological approaches are used to obtain such materials: foaming of liquid metals [1], laser [1,2] or electron beam 3D printing with metallic powder [3], powder metallurgy method including removable space holders [4–8]. The last method is the simplest and most versatile, allowing the obtaining of materials with porosity exceeding 80%, high specific strength, and sufficient fracture strain under different strain rates.

Concerning titanium and titanium-based porous materials, early works were devoted to the production of porous titanium using NaCl as a space holder [5,9,10,11]. These studies were carried out either on hydrogenated/dehydrogenated titanium powder [9] or globular powder [8] sintered at relatively low temperatures (780 °C), which correlated well with the physical and mechanical properties of cancellous bones and was promising for use in implants. Noteworthy are the works [10,11], in which, in addition to aluminum powder, other than NaCl space holder was used, ensuring the formation of highly porous Ti-Al intermetallic compounds. The latter works can be mentioned separately because they describe a technological approach uniting an exothermic reaction between Ti and Al powders as a material synthesis method with the application of calibrated NaCl crystals as a removable space holder to form the specific porosity. The mechanical behavior of porous materials is determined with specified porosity parameters, including total volume content, size of pores, uniformity of their distribution, and, of course, the properties of the basic metallic material [1,8,9]. Thus, to achieve anticipated strength, ductility level, and dumping capacity, the parameters of pore structures should be strictly controlled. In the previous work, such detailed analysis was done for commercial purity titanium with various porosity and manufactured with use of different technological approaches [12]. It was shown that the best properties are provided by porous titanium, which was obtained by sintering titanium hydride and using ammonium carbonate ($(NH_4)2CO_3$) – thereafter indicated as AC) as a space holder [13].

However, due to the fact that commercial-purity titanium (c.p.Ti) has a relatively low level of strength, which means that

in its porous form, its energy absorption capacity is inferior to titanium-based alloys.

That is why the aim of the present work was the fabrication of highly porous titanium-based and widely used Ti-6(wt.%)Al-4V alloy using earlier developed powder metallurgy approaches based on the usage of hydrogenated titanium (titanium hydride) [14,15] and ammonium bicarbonate as a space holder [12]. In this approach, hydrogen is emitted from hydrogenated titanium powders during vacuum heating. Atomic hydrogen emitted on $TiH_2$ decomposition cleans the powder surfaces, thus reducing the content of impurities (O, N, C) in sintered material. Also, dehydrogenation is accompanied by a noticeable decrease in material volume (linear shrinkage up to 6.7%), resulting in a highly defective crystal structure and activated sintering of dehydrogenated powder particles. Moreover, the shrinkage of particles on dehydrogenation can be used as an additional factor to affect the porosity of sintered powder compacts. So, the aim of the present study was to obtain desirable porous Ti-6Al-4V structures and investigate the mechanical behaviors of produced material under conditions of quasi-static and dynamic compression in order to evaluate their potential for energy absorption.

## 2. MATERIALS AND METHODS

### 2.1. Material specimen preparation.

Two types of porous Ti-6Al-4V samples were prepared via earlier developed press-and-sinter Blended Elemental Powder Metallurgy (BEPM) approach using titanium hydride (Fig. 1a) and 60%Al-40%V master alloy (Fig. 1b) as raw powders. For the first type of samples, these powders (size less than 100 µm) were blended with AC particles (Fig. 1d) as removable space holders [12,13], and next, the powder mixtures were compacted at room temperature (300 MPa). The AC was preliminary evaporated from the compacts on heating in the open air up to 150 °C, then the powder compacts were sintered under vacuum (1250 °C, 4 h) to produce uniform porous Ti64 alloy [14,15] (hereafter named Ti64BEPM). During the vacuum sintering, hydrogen and the AC remnants were removed from the material.

To produce the second type of samples, Ti64 alloy sintered using above-described protocol but without the AC additions, was hydrogenated again and crushed to obtain hydrogenated pre-alloyed Ti-6Al-4V powder (later named Ti64PA) (Fig. 1c). The produced Ti64PA powder (less than 100 µm in size) was blended with the AC. The Ti64PA+AC powder blend was compacted, heated to evaporate AC and finally sintered under vacuum following the above-described procedure to obtain porous Ti64PA material [16]. To achieve various porosity of sintered Ti64BEPM and Ti64PA materials, the amount of AC in the green compacts was varied in the range of 50, 75, and 100 volumes % relatively volumetric amount of metallic powders. More details on the method mentioned above are given in [12], where porous c.p.Ti material was produced using AC in the amount from 25 to 75 volumetric %. In the present work, porous c.p.Ti samples were also sintered using titanium hydride powder blended with 100 vol.% of AC to compare their characteristics with those of porous Ti64BEPM and Ti64PA materials manufactured with the same AC content.

All sintered materials had initial dimensions of 12×12×60 mm, from which cubic samples with an edge size of 10 mm were then cut out for microstructural studies. Some typical characteristics of the sintered samples are listed in Table 1. Cylindrical samples with gauge length and diameter of 10 mm for direct impact Hopkinson pressure bar (DIHPB) and quasi-static compression (QSC) tests were cut out by the electric discharge machining technique.

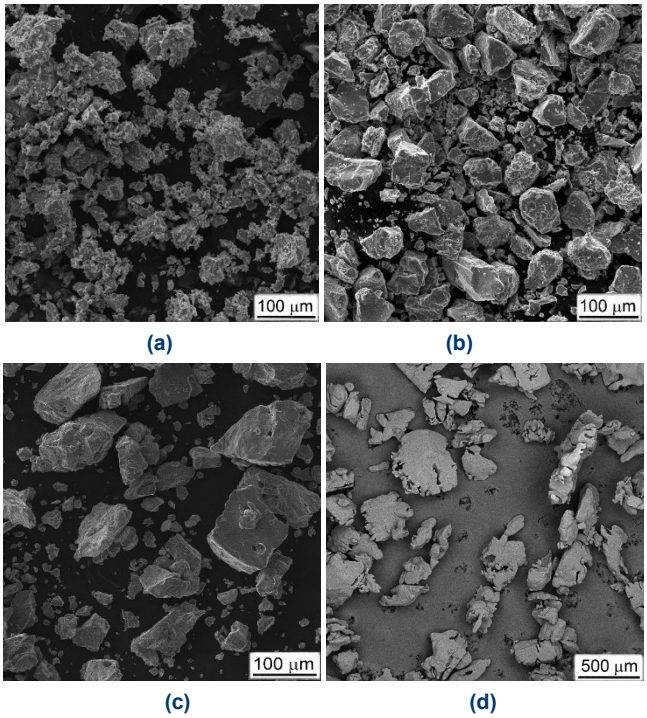


**Fig.1.** Powders used for preparation of porous Ti-6-4 materials: (a) TiH2, (b) V-Al master alloy, (c) pre-alloyed Ti-6-4 powder, (d) Ammonia Carbonate. SEM, (a, b) SE, (c) BSE

**TABLE 1.** Some characteristics of sintered porous samples

| ## | Sample type | Average density [g/mm$^3$] | Porosity [%] | Relative density [-] | Densification strain [-] |
|---|---|---|---|---|---|
| 1 | Ti64BEPM+50%AC | 2.197 | 50.4 | 0.50 | 0.50 |
| 2 | Ti64BEPM+75%AC | 1.929 | 56.5 | 0.44 | 0.56 |
| 3 | Ti64BEPM+100%AC | 1.824 | 58.8 | 0.41 | 0.59 |
| 4 | Ti64PA+50% AC | 1.992 | 55.0 | 0.45 | 0.55 |
| 5 | Ti64PA+75% AC | 1.882 | 57.5 | 0.42 | 0.58 |
| 6 | Ti64PA+100% AC | 1.455 | 67.2 | 0.33 | 0.67 |
| 7 | Ti+100%AC | 1.443 | 65.8 | 0.31 | 0.62 |

### 2.2. Experimental procedures.

The first type of strength experiments, e.g., dynamic tests, were performed using the split Hopkinson pressure bar technique (SHPB) (Fig. 2a). In turn, standard quasi-static compression strength tests were carried out on the MTS C45 universal testing machine (the strain rate used: $10^{-3}$ $s^{-1}$).

The laboratory system presented in Fig. 2a [12] is a modification of the classic SHPB system called the forward direct impact Hopkinson pressure bar (forward-DIHPB), which allows the deformation of the specimen to large strains (up to densification in the case of cellular solids) [16,17]. The design solution of the DIHPB arrangement is similar to the one presented in [18]. The currently used laboratory stand consists of a striker bar with a diameter of 36 mm and mass of 4760 g launched from a gas gun and a 6 m long output bar, i.e., two connected 3 m long pressure bars with a diameter of 40 mm and a data acquisition system. The specimen is put at the front of the output bar, and the 600 mm long striker bar can directly impact the specimen. The striker bar and output bars are made of the same material, i.e., C45 steel, with a yield strength and elastic wave velocity equal to 735 MPa and 5140 m/s, respectively. To determine force/stress on the loading surface of the specimen, a pair of strain gages placed 500 mm from the front end of the output bar is used to record transmitted signals. The position of strain gages and length of the output bar were chosen so as to avoid wave superposition.

nominal strain can be calculated as done in quasi-static tests. The impact velocity in dynamic tests varied slightly within the range from 14.2 to 15 m/s, which, taking into account the dimensions of the tested samples, corresponded to a strain rate of approximately 1420-1500 $s^{-1}$.

It should be noted here that stress and strain are calculated in a standard way as in the case of solid materials, i.e., in relation to the initial cross-section and initial length of the sample (calculation of nominal stress and nominal strain). However, in the case of porous (cellular) materials, when their density changes during deformation, the actual values of stress and strain occurring in the walls of the porous material differ significantly from those calculated using standard procedure. Therefore, in order to emphasize this difference, the terms "apparent stress" and "apparent strain" will be used in the rest of this paper.

Material microstructures before and after tests (on the surface of cross-sections that were made along the red lines indicated in Fig. 2c), as well as the specimens' fractures, were studied using scanning electron microscopes (SEM), Vega 3

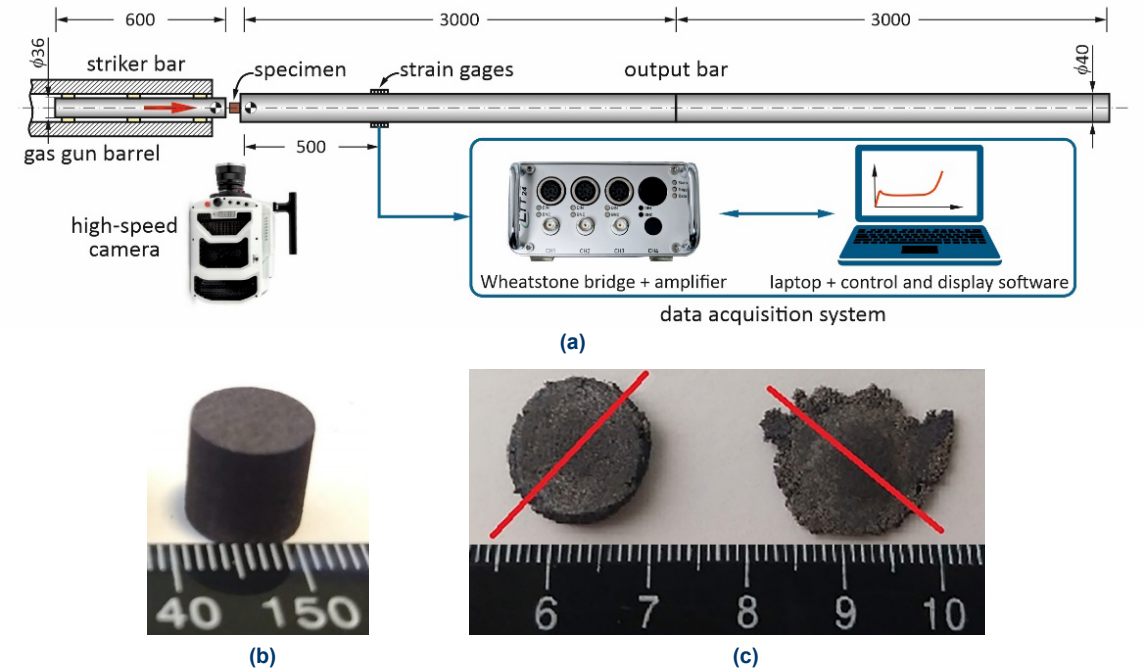


**Fig.2.** Scheme of the SHPB apparatus used for dynamic strength tests [12] (a), general view of the samples before (b) and after the DIHPB tests (c) - the red lines represent the planes along which the tested samples were cut for fractographic and metallographic examinations

Phantom V1612 high-speed camera (Vision Research, Inc., Wayne, NJ, USA) was used to measure the compression rate and to identify failure modes, as well as to confirm that the striker bar kinetic energy was sufficient to provide a near-constant compression velocity of specimen up to a nominal strain of at least 0.5. High-speed video images were recorded with a resolution of 512×208 pixels and a frame rate of 110,000 fps. Crush test markers and specialized TEMA Classic software (Image System AB, Linköping, Sweden) were used to ensure high measurement accuracy based on video images. The impact velocity and the deformation length history of specimens were determined by subtracting the displacements between the projectile and output bar. Thus, the corresponding

and Mira 3 (Tescan, Czech Republic), equipped with energy dispersive X-ray (EDX, Bruker, Germany in Vega 3, or Oxford Instruments, UK in Mira 3, respectively) spectroscopy allowing the measurement of the chemical composition of materials.

## 3. RESULTS

### 3.1. Microstructure observation

Microstructures of sintered samples, including some features inside the pores, are presented in Fig. 3. It is clear that pores have a somewhat irregular shape (Figs. 3a, c, e, g, k) that reflects the shape of the AC particles (Fig. 1d). As for the features of the internal structure of the pores, regardless of the

amount of the used space holder, they are characterized by the formation on the inner surface of fragments with a hexagonal structure typical for the h.c.p. symmetry of the α-phase (Fig. 3b, d, f, h, j, l).

As for porous c.p.Ti, it was generally characterized by the similar structure of pores (Fig. 3m). However, the inner pore has a smoother surface, and the hexagonal structure is revealed only at much higher magnifications (Fig. 3n). This is quite typical for such a material and was described in detail earlier [12]. Despite the measured difference in volume fraction of pores (Table 1) depending on the amount of AC additions and method of Ti64 matrix manufacturing (BEPM or PA), a comparison of these samples did not reveal principal differences in their microstructure (Fig. 3). The outer surfaces of the samples did not display any apparent differences even in the number of pores (Figs. 3a, c, e, g, i, k).

Comparing the internal surfaces of the pores of samples obtained by the BEPM or PA method, it can be noted that in the

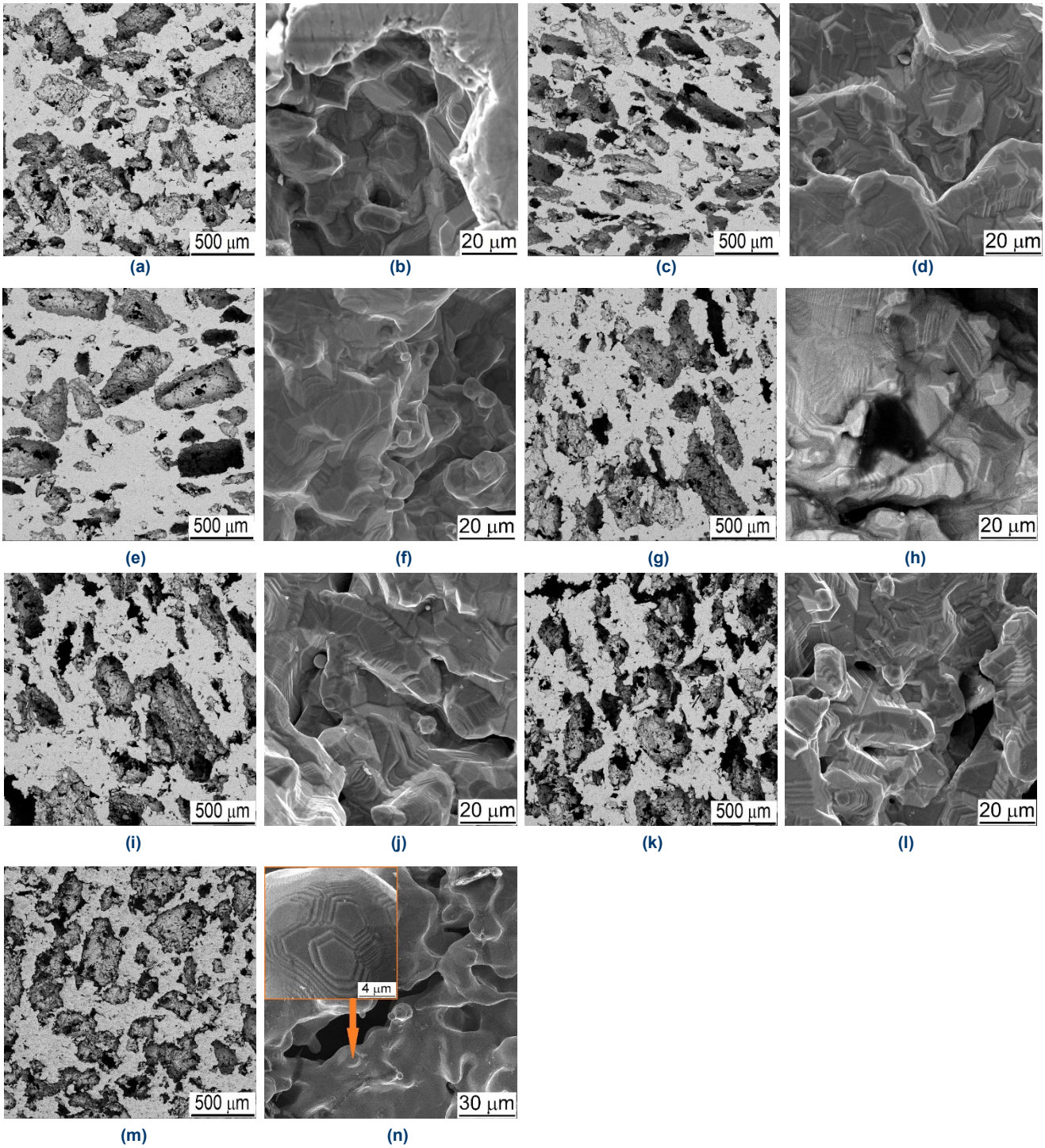


**Fig.3.** Microstructure of sintered samples prepared via (a-f) BEPM method, and (g-l) using pre-alloyed powder in the initial (sintered) state. Content of AC: (a, b, g, h) 50%, (c, d, l, j) 75%, (e, f, k, l) 100%; (m, n) Ti100AC. SEM, (a, c, e, g, i, k, m) – side views, BSE; (b, d, f, h, j, l, n) – inner structure of pores, SE

latter case, the formation of hexagonal shape reliefs on the internal surface is slightly pronounced (compare Figs. 3b, d, and f with Figs. 3h, j, and l). It could be due to more developed processes ensuring the formation of surface planes with lower surface energy during two sintering stages (sintering of BEPM compacts at the first stage and then sintering of PA powder compacts).

The structure of the Ti64 alloy in both variants (BEPM and PA) can be described as two-phase α+β with lamellar morphology of both phases (Fig. 4) that is the typical microstructure of sintered Ti64 alloy obtained with powder technologies [14] and similar to that obtained with as-cast technology [19]. The microstructure of porous titanium of commercial purity was typical of such a material and was described in detail earlier [12].

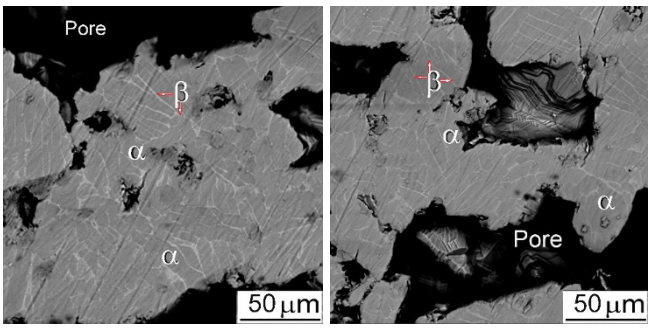


**Fig.4.** Microstructure of metallic base of porous Ti-6-4 prepared with (a) BEPM, and (b) PA approaches. SEM, SE

### *3.2.* Mechanical characterization.

In contrast to the similar porous microstructure, the mechanical behavior of materials obtained by different methods differed significantly. Fig. 5 shows the results of quasi-static strength tests of such samples. First, it should be noted that the strength levels of porous Ti64 samples depend on the manufacturing approach. All Ti64BEPM materials generally demonstrate a noticeably higher level of compression strength (up to 500-800 MPa, Fig 5a) than that of Ti64PA materials (not higher than 140 MPa). Moreover, Ti64BEPM samples manufactured using a blend of TiH2 and V-Al master alloy samples demonstrate smooth stress-strain curves having a gradually increasing character, similar to porous titanium, obtained by the same method (Fig. 5a). A minor exception is the stress-strain curve of the sample prepared using 50% AC, which is probably due to some heterogeneity in the distribution of pores throughout its volume.

The difference between the samples having different porosities (made with various amounts of space holder AC) consists in the level of compressive strength achieved, which naturally decreases as porosity increases. It is also clearly visible that with the same porosity, which is also reasonably expected, the Ti64 alloy has a higher strength compared to pure Ti (compare curves 1 and 2 in Fig. 5a). In contrast, the porous material obtained by the second method using pre-alloy powder behaves completely differently during quasi-static compression (Fig. 5b) - samples of all three porosities have a peak strength at the initial stage of compression, after which a significant drop in strength is observed. This drop is the greater, the lower the porosity of the sample and the greater the strength of the first deformation stage. It is quite an unexpected fact that after such a drop (with a visible deformation of approximately 0.3-0.5), all samples had approximately the same strength, which was more than half as strong as that of porous pure titanium (compare curve 1 with curves 2-4 in Fig. 5b).

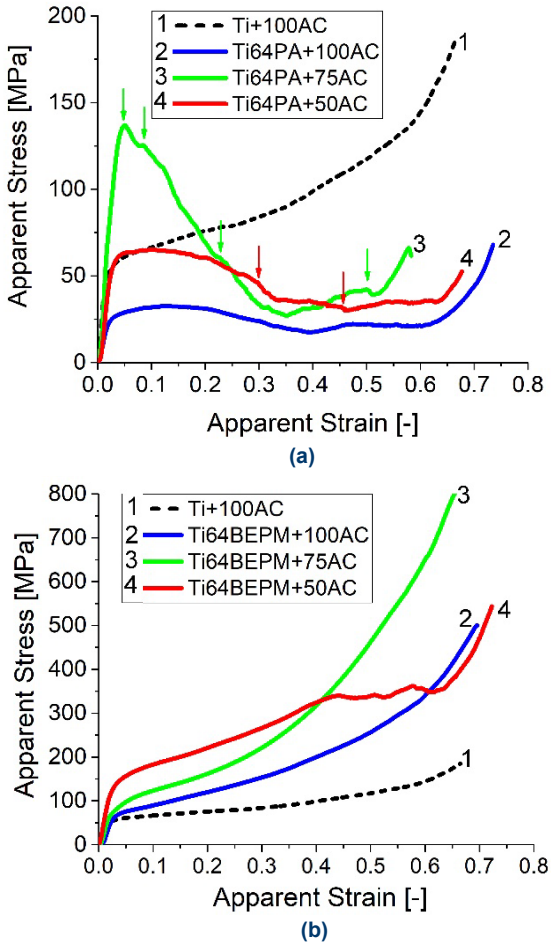


**Fig.5.** Apparent stress- apparent strain curves for quasi-static compression tests (strain rate $10^{-3}$ $s^{-1}$) of porous Ti+100%AC and Ti64 obtained via BEPM (a) and AP (b) approaches prepared with different amount of AC

In turn, Fig. 6 presents a comparison of the results of dynamic compression tests (DIHPB) for pure titanium (a) and Ti64 (b) samples with different porosities that were impacted with approximately the same impact velocity of the striker bar. As for porous pure Ti, the material tested in this work after using 100% AC completely fits the previously obtained trend in the work [12] when higher porosity resulted in a decreased strength level (Fig. 6a). In turn, Figure 6b shows the curves of dynamic compression tests for all types of porous Ti64. It should be noted that, in contrast to quasi-static compression, all BEPM and PA samples showed smoothly increasing curves without any extrema or inflections during dynamic tests. The significant advantage of BEPM-type samples over PA-type samples is clearly visible (compare curves 1-3 with curves 2-6 in Fig. 6b). Insight into the mechanical behavior of the tested materials under dynamic loading conditions is also provided by the high-speed camera images presented in Fig. 7.

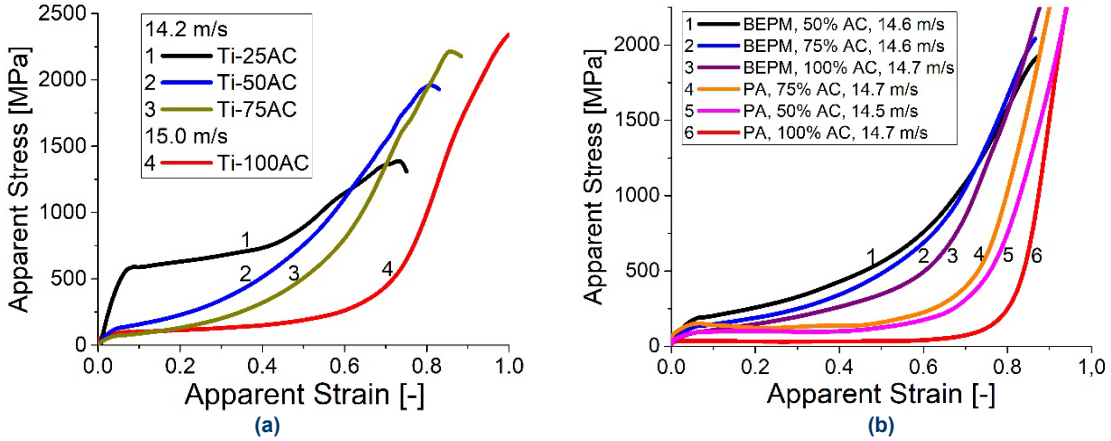


**Fig.6.** Dynamic apparent stress- strain curves of the porous samples produced using various AC amounts: (a) porous c.p.Ti (curves 1-3 in (a) are taken from previous work [12], curve 4 present study), and (b) porous Ti-6-4 alloy prepared via BEPM (curves 1-3), or PA (curves 4-6) approaches


**Fig.7.** Frames taken from video records of DIHPB tests of: (a) Ti+100AC; (b) Ti64BEPM+50AC; (c) Ti64BEPM+75AC; (d) Ti64BEPM+100AC; (e) Ti64PA+50AC; (f) Ti64PA+75AC; (g) Ti64PA+100AC (Red arrows in (e,f,g) indicates appearance of brittle cracks)

Porous c.p.Ti (Fig. 7a) and porous Ti64 obtained by the BEPM method (Figs. 7b-d) are characterized by the sufficient plastic deformation mode and do not collapse brittlely until the very end of the crushing. In contrast, porous Ti64 samples obtained by the PA method began to crack brittlely approximately halfway through the compression process and were almost entirely destroyed by the end of the dynamic compression (Figs. 7e-g). Analysis of these video records, especially taking into account presented in Figs. 6a and b data, allows to conclude that BEPM porous Ti64 samples are relatively ductile, similar to pure Ti ones, while PA porous Ti64 samples have somewhat brittle behavior. Under dynamic crash conditions, crack initiations observed in the video frames do not manifest themselves as characteristic points on the stress-strain curves (Fig. 6b). But the stress "jumps" observed on the stress-strain curves under quasi-static compression (marked with the corresponding red and green arrows in Fig. 5b) are most likely caused by such brittle cracking of the samples.

## 4. DISCUSSION

### 4.1. Energy absorption capacity.

A detailed analysis of the test results should be carried out for a realistic assessment of the potential of porous Ti64 obtained by the powder metallurgy methods used in this work in terms of energy absorption efficiency. Fig. 8 shows a pairwise comparison of the results of quasi-static tests of samples of two different types (BEPM and PA), obtained using the same amount of space holder, as a result of which they had close porosity levels (Table 1). It is clear for each pair that the stress-strain curves of the BEPM samples are always higher, which is a characteristic feature indicating a greater strength of BEPM materials. However, there is a certain horizontal section on the curves for PA-type samples, which is considered a positive feature for energy-absorbing materials [1,6,12,20].

A similar difference occurs in the case of dynamic tests using the DIHPB method (Fig. 9). All curves for Ti64PA samples lie below the curves of both Ti64BEPM and pure porous Ti for all the used volumes of the AC space holder. Also, stress-strain curves for Ti64PA materials have a large horizontal section (plateau). It is worth noting that the curves for Ti64BEPM and porous Ti at 50% AC and 75% AC almost coincide with each other (Fig. 9a and b), while at 100% AC the Ti64 curve is noticeably higher (Fig. 9c).

The results of dynamic DIHPB tests were recalculated in the dependencies of specific energy absorption (SEA) vs. strain for all types of samples (Fig. 10a). Analyzing the given dependences, we can conclude that porous Ti64 samples form two groups of curves depending on the type of manufacturing process. Thus, all curves for porous material of the BEPM (curves 2-4 in Fig. 10) type lie significantly higher than the curves of the PA type (curves 3-7), while the curve for porous Ti with 100% AC (curve 1) separates these two groups. It can also be noted that the difference in the SEA between these two types of samples increases with increasing deformation (Fig. 10b). For instance, for strain 0.4, the difference in SEA between their highest level for Ti64BEPM and Ti64PA does not exceed 2.5 times, while for strain 0.8 the difference increases to approximately four times on average.

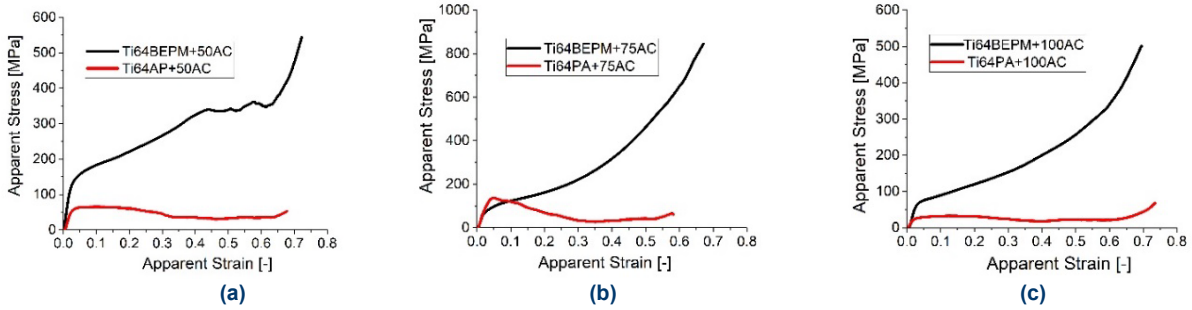


**Fig.8.** Apparent stress- strain curves for quasi-static compression tests (strain rate $10^{-3}$ $s^{-1}$) of porous Ti64 prepared with AP and BEPM approaches and addition of: (a) 50%AC, (b) 75%AC, and (c) 100%AC

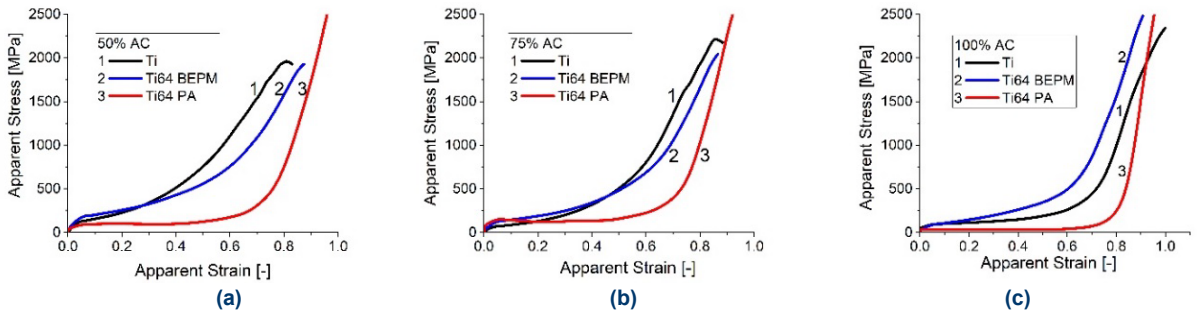


**Fig.9.** Comparison of dynamic compression curves for porous Ti (curves 1) and Ti64 (2, and 3) prepared by two different ways (2 – BEPM method, 3 – using pre-alloyed powder) depending on amount of space holder (Ammonia Carbonate - AC): (a) – 50%, (b) – 75%, (c) – 100%. Data for porous Ti obtained with additions of 50% and 75% ammonia carbonate in (a) and (b) were taken from previous work [12]

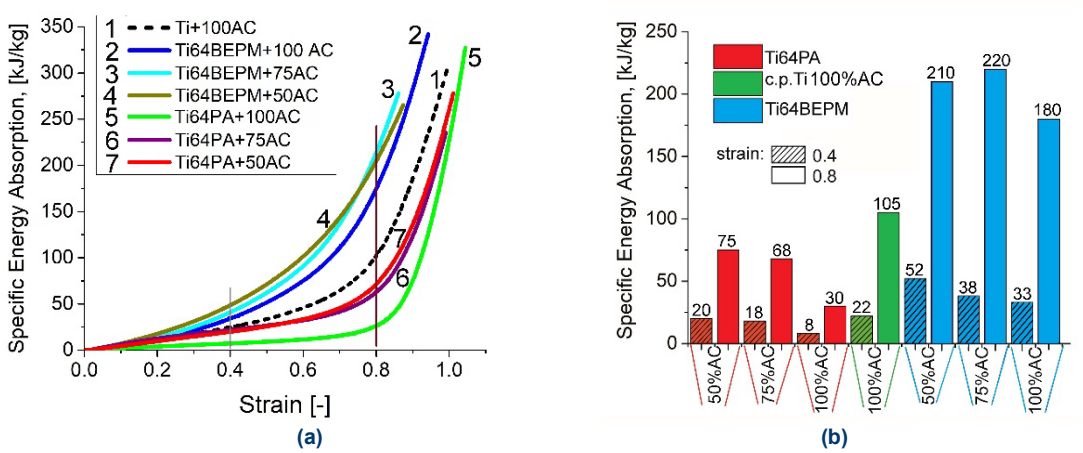


**Fig.10.** Comparison of specific energy absorption at dynamic compression for all studied porous materials: (a) – specific energy absorption vs. strain curves, (b) – specific energy absorption for strain 0.4 and 0.8

### 4.2. Fractographic analysis.

To determine the nature of such differences in the mechanical behavior of porous Ti64 obtained by different methods, an analysis of the fractured surfaces and microstructure of the metal after dynamic DIHPB tests was carried out (Fig. 11 and 12). A common feature of all the tested samples is almost completely collapsed and deformed pores due to plastic deformation α- and β- phase plates (for example – Figs. 11b, f, and Fig.12 d). It is possible to note a certain difference in the structure of the fracture surfaces of samples Ti64BEPM and Ti64PA - in the latter case, these surfaces had smaller fragments and some evidence of a tendency to brittle fracture (for example, compare Fig. 11a and Fig. 12e).

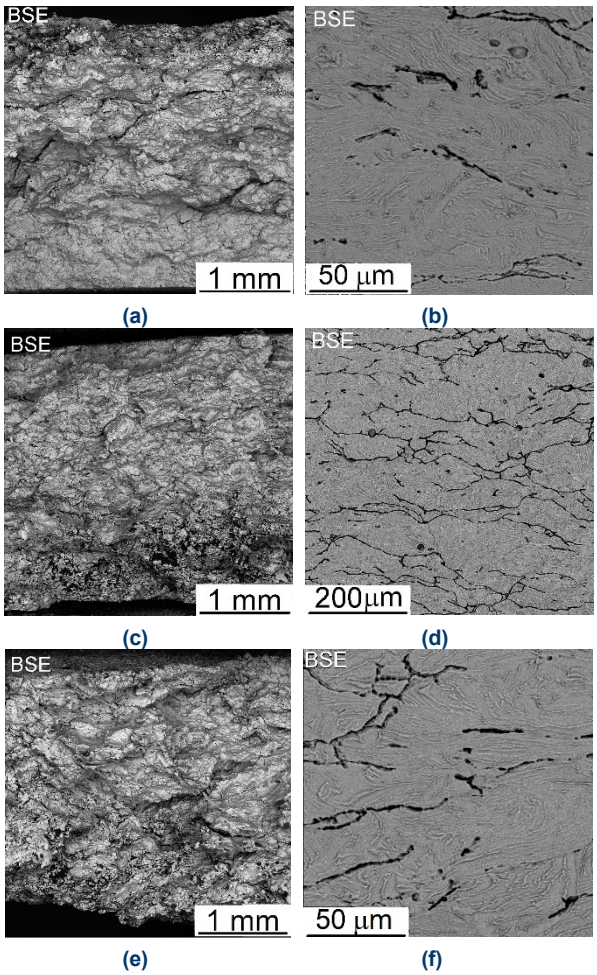


**Fig.11.** Fracture surfaces (a, c, e) and microstructure (b, d, f) of porous Ti64BEPM samples after DIHPB tests. Amount of AC in the initial mixture: (a, b) 50%; (c, d) 75%, (e, f)100%. (a, c, e) fractured samples, (b, d, f) ground and polished metallographic sections. SEM

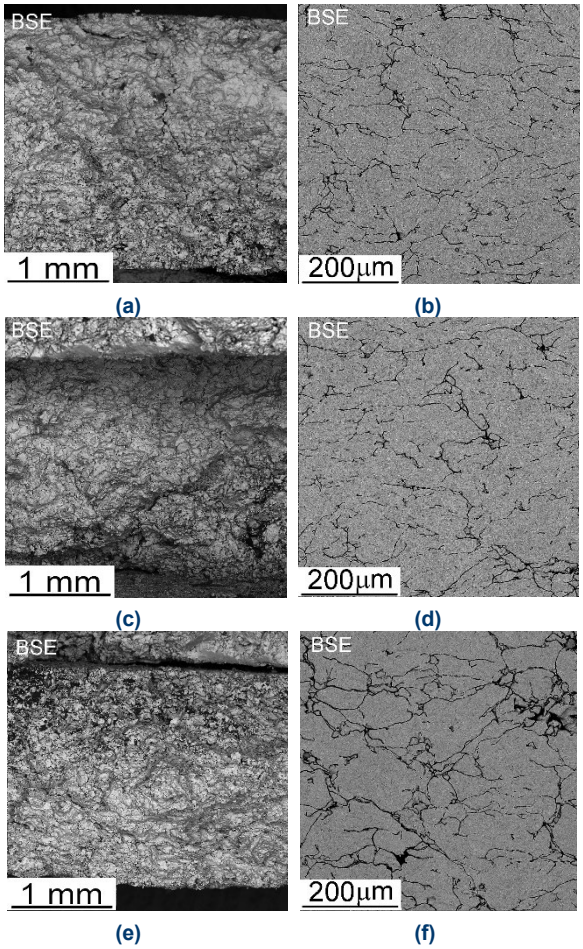


**Fig.12.** Fracture surfaces (a, c, e) and microstructure (b, d, f) of porous Ti64PA samples after DIHPB tests. Amount of AC in the initial mixture: (a, b) 50%; (c, d) 75%, (e, f)100%. SEM

In the case of porous Ti100AC samples, they were characterized by a very ductile fracture surface (Fig. 13a) and, due to the single-phase α-state (h.c.p.), the absence of a visible

substructure on the section densified after the compression test (Fig. 13b).

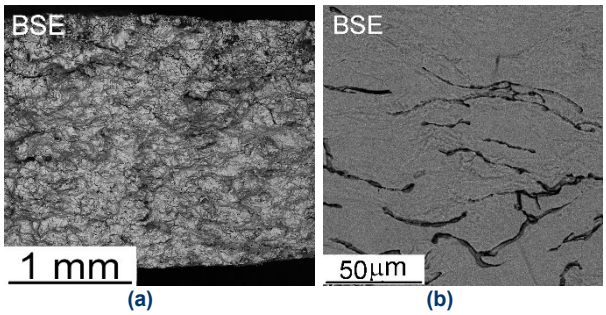


**Fig.13.** Fracture surfaces (a) and microstructure (b) of porous Ti100AC samples after DIHPB

Thus, the study of the microstructure of the samples both in the initial state and after testing, as well as their fractures, does not give an unambiguous conclusion about the nature of such a significant difference in their mechanical behavior when tested in compression. It is well known that differences in alloying element content and specific impurities, which are inevitably presented in alloys produced with powder approaches, noticeably affect their mechanical characteristics. Therefore, a more detailed study of chemical composition was carried out for metal matrixes and pore surfaces in initial sintered conditions and after the deformation tests.

### 4.3. Chemical composition analysis.

Table 2 shows the results of EDS analysis for two extreme cases with 50% AC and 100% AC for sintered samples Ti64BEPM and Ti64AP. It is evident that the composition of α- and β-phases is rather typical of a commercial Ti64 alloy [18,20,21]. Some increased oxygen and carbon contents (usually within 1.5-3.5%) measured on the polished surfaces are also typical due to the adsorption of these elements from the environment during the sample's preparation. Usually, the surface content of these impurities is approximately an order of magnitude higher than the one in the depth of titanium alloys. Earlier results for titanium alloys produced with the BEPM approach using a titanium hydride powder [14,15] revealed that the content of these impurities is within 0.15-0.24 O and 0.05-0.07%C, i.e., it met the general requirements for commercial titanium alloys. Therefore, the admissible volume content of these impurities in sintered BEPM and PA materials in the present research can be assumed. At the same time, a noticeably increased content of impurities (O up to 26.9%, C up to 11.9%) was observed in inner pore surfaces (Table 2). Such obvious contamination of inner volumes of pores can be explained by the remnants of AC evaporated during the used regimes of pore-holder removing and vacuum sintering.

Local chemical analyses of the samples after DIHPB tests are presented in Fig. 14 and Table 3 (Bruker system). First of all, it is necessary to mention that the data analysis of the chemical element content measured by EDS analysis data displays the content of these elements not only on the analyzed surface but in the surface layer with a depth of about 3 microns [22].

**TABLE 2.** Local chemical composition of the α- and β-phases, as well as of pore surfaces in the samples in the initial state (made with Oxford Instruments EDS)

| ## | Sample type | Phase | Average content of elements, wt. % | | | | |
|---|---|---|---|---|---|---|---|
| | | | Ti | Al | V | O | C |
| 1 | Ti64BEPM+50%AC | α | 84±0.9 | 7.3±0.8 | 2.3±0.1 | 1.8±0.4 | 2.9±0.14 |
| 2 | | β | 74±0.4 | 4±0.08 | 16.1±0.4 | 1.5±0.5 | 3.6±0.28 |
| 3 | | **Pore** | **66±3.5** | **5.2±0.3** | **6.1±0.5** | **14.4±3.3** | **9.2±1.92** |
| 4 | Ti64BEPM+100%AC | α | 85±0.97 | 7.1±0.45 | 2.3±0.15 | 2.6±0.66 | 2.6±0.12 |
| 5 | | β | 74±0.65 | 5.4±0.29 | 16±0.82 | 1.5±0.23 | 3.5±0.22 |
| 6 | | **Pore** | **71±0.69** | **4.8±0.35** | **6.6±0.50** | **12±0.75** | **5.8±1.49** |
| 7 | Ti64PA+50% AC | α | 84±3.22 | 6.3±0.87 | 2.9±0.14 | 0.9±0.55 | 2.9±0.20 |
| 8 | | β | 67±2.43 | 6.4±0.27 | 12.1±0.85 | 1.5±1.12 | 10.1±1.86 |
| 9 | | **Pore** | **59±2.76** | **5.8±0.78** | **5.8±0.72** | **23.2±3.42** | **9.8±1.18** |
| 10 | Ti64PA+100% AC | α | 86±2.74 | 6.4±0.47 | 2.3±0.21 | 1.7±0.55 | 3.1±0.42 |
| 11 | | β | 75±2.71 | 3.5±0.17 | 14.6±1.89 | 3.3±0.93 | 3.5±0.85 |
| 12 | | **Pore** | **53±2.83** | **5.1±0.76** | **2.7±0.55** | **26.9±8.52** | **11.9±1.33** |

The redistribution of alloying elements and impurities after deformation is similar to that for initial sintered materials. Naturally, the general laws of alloying element (Al, V) redistribution between the α and β phases are quite similar to those for sintered BEPM and PA materials. The acceptable content of iron impurity was localized in the β phase. The content of O and C impurities at polished surfaces and in the layer of about 3 microns thick generally corresponds to those for initial materials, despite the increased carbon content (7-12%) observed in some locations at the β phase. It can be explained by the localization of carbon impurity in areas adjacent to studied locations. Similar to sintered alloys, significantly increased carbon (up to 30-40%) and oxygen (up to 15%) contents were observed at the surfaces of deformed pores. These results suggest a slight influence of impurities in material volume and a slight influence of pore-holder remnants at pore surfaces on the entire deformation behavior of produced porous materials.

**TABLE 3.** Local chemical composition of the α- and β-phases in the samples in the state after DIHPB tests (made with Bruker EDS)

| ## | Point # | Content of elements, wt. % | | | | | | |
|---|---|---|---|---|---|---|---|---|
| | | Ti | Al | V | Fe | C | O | N |
| Sample Ti64PA100; Location of points in Fig. 14a | | | | | | | | |
| 1 | 1 (beta) | 83.23 | 5.07 | 3.80 | 0.38 | 7.05 | 0.47 | 0.00 |
| 2 | 2 (alpha) | 90.25 | 5.78 | 0.51 | 0.00 | 2.28 | 3.08 | 0.00 |
| Sample Ti64PA50; Location of points in Fig. 14d | | | | | | | | |
| 3 | 1 (beta) | 81.81 | 3.94 | 9.66 | 0.90 | 12.07 | 0.00 | 0.00 |
| 4 | 2 (alpha) | 90.84 | 9.25 | 0.66 | 0.01 | 8.54 | 0.25 | 0.00 |
| Sample Ti64BEPM100; Location of points in Fig. 14g | | | | | | | | |
| 5 | 1 (beta) | 81.15 | 5.02 | 11.13 | 1.06 | 1.60 | 0.03 | 0.00 |
| 6 | 2 (alpha) | 89.57 | 7.38 | 1.48 | 0.08 | 1.11 | 0.40 | 0.00 |
| Sample Ti64BEPM50; Location of points in Fig. 14j | | | | | | | | |
| 7 | 1 (beta) | 86.64 | 5.80 | 3.24 | 0.20 | 3.16 | 0.96 | 0.00 |
| 8 | 2 (alpha) | 89.19 | 6.90 | 1.59 | 0.06 | 1.42 | 0.84 | 0.00 |

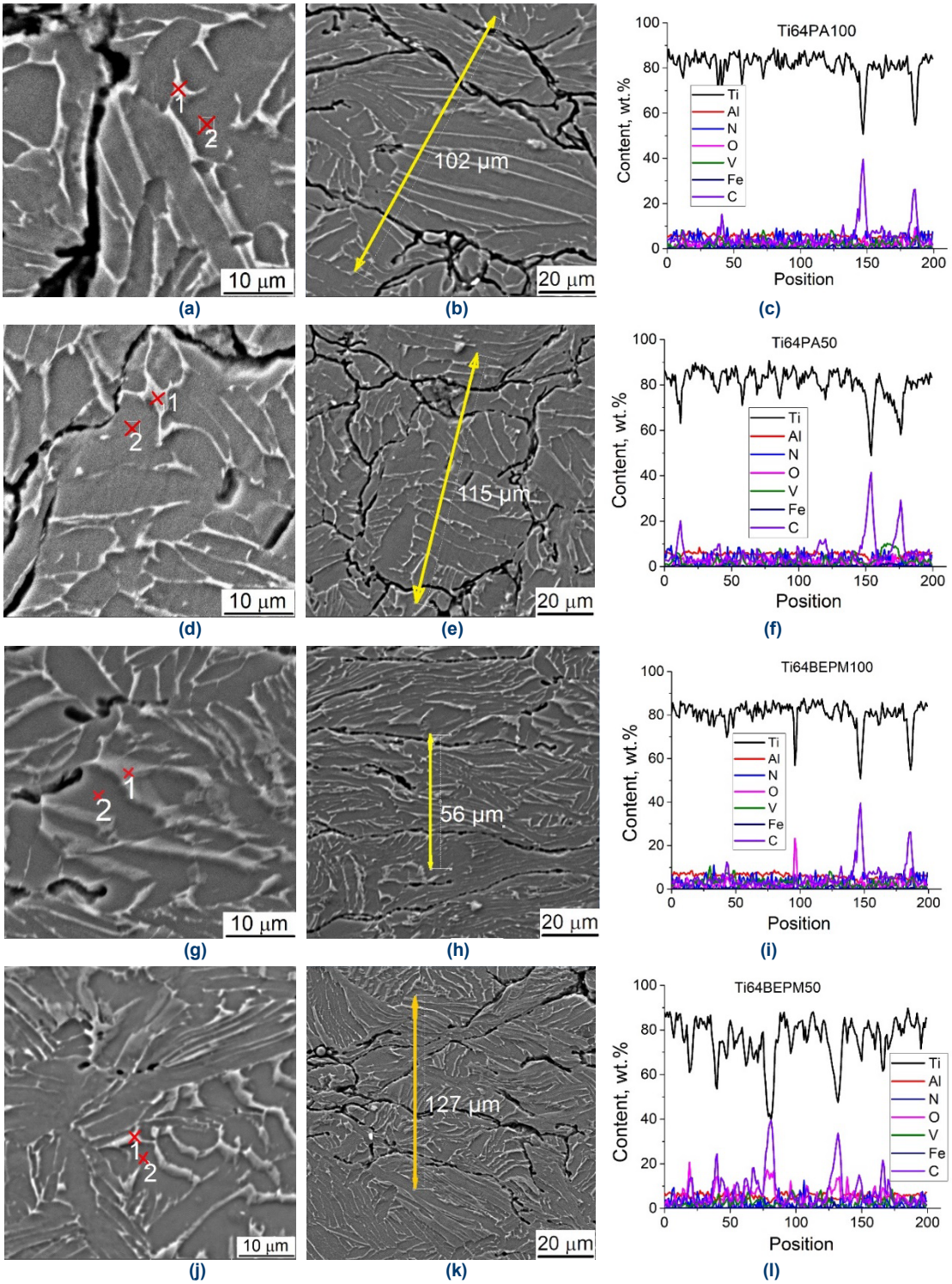


**Fig.14.** Images (a,b,d,e,g,h,j,k) SEM, and chemical elements distibutions in the samples (a-c) Ti64PA100, (d-f) Ti64PA50, (g-i) Ti64BEPM100, (j-l) Ti64BEPM50 after compression test. Points in the Figs. (a, d, g, and j) corresponds locations where local chemical analysis was made (see Table 3). Lines in Figs. (b, e, h, and k) indicate positions, where distributions of elements were measured (Figs. c, f, i, and l)

This difference in the absorbed oxygen and carbon content causes some differences in the details of the fracture surfaces of the Ti64BEPM and Ti64PA samples (Fig. 15a and 15b, respectively). It can be assumed from a comparison of these two micrographs that in the latter case, the fracture surface has more apparent signs of embrittlement, which is expressed in the fact that areas of the Ti64 alloy look less deformed, and there are separate chip facets on their surface (Fig. 15b vs. 15a). Since, as shown above, it is the pore surface that is most saturated with contaminating elements (Figs. 14 and Table 3), then it can be expected that destruction is initiated in certain areas of such pore surfaces where the highest local stresses arise.

So far, various studies have been conducted on the mechanical properties of porous Ti and Ti6Al4V structures. For example, in the work [23] in which porous Ti was produced with NaCl as a space holder, it was shown that maximum

compressive strength under quasi-static loading monotonically decreases from 470 MPa to 130 MPa with an increase in porosities from 36% to 60%. In turn, presented in work [24], the Ti6Al4V alloys with 41 to 64% porosity obtained by using powder magnesium as a space holder were characterized by a quasi-static compressive strength ranging from 172 MPa to 40 MPa.

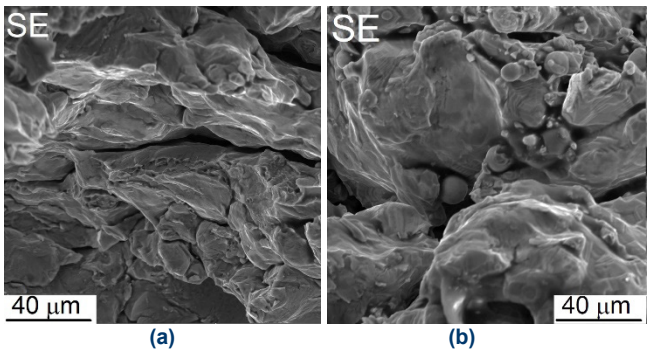


**Fig.15.** Details of fracture surfaces in the DIHPB tested samples prepared with 100%AC: (a) Ti64BEPM, (b) Ti64PA. SEM.

Comparing the above-mentioned results with our research presented in [12] and this work results, it should be stated that the application of titanium hydride and ammonium carbonate (BEPM technology) allows obtaining porous Ti-based materials with high mechanical properties and energy absorption capacity, via simple sequence of mixing, pressing, and sintering. In the case of the porous Ti, Ti+100AC compressive strength – (see Fig. 5a) is approximately twice as high as the compressive strength of an analogous porous material presented in the work [23]. Moreover, the Ti+100AC material exhibits excellent plastic properties and densification ability. This is evidenced by the smooth profile of the compression curve until densification is achieved at a strain of approximately 0.6, whereas the porous materials presented in work [23] crack at strains ranging from 0.05 to 0.08.

Similarly, the Ti6Al4V alloy produced by the BEPM technology has high mechanical properties. Compared to the analogous alloy presented in [24], our porous Ti64BEPM achieves approximately 45% higher compressive stress levels at the same strain value (see Fig. 5b and Fig 8). What is particularly worth emphasizing is that the compression and densification process of the Ti64BEPM porous material under quasi-static loading conditions, as well as under dynamic compression, occurs stably, i.e., the profile of the compression curve is smooth without visible irregular stress drops and rises. An exception here is the Ti64BEPM+50%AC material, in which irregular changes in the stress profile occur when the strain exceeds approximately 0.4. This indicates slightly worse plastic properties and densification ability of the Ti64BEPM+50%AC material compared to the other tested BEPM materials. However, when compared to the results presented in [24], in which the tested materials with similar porosity showed stress drops at strain ranging from 0.04 to 0.05, it should be stated that the Ti64BEPM+50%AC material reveals relatively higher mechanical properties.

It is also worth emphasizing at this point that our porous material is much cheaper, considering the initial powders' cost and the manufacturing technology's complexity.

## 5. CONCLUSIONS

The obtained results allow us to conclude the following:

1. Ti-6Al-4V alloy having controlled porosity within the 50-67% range was manufactured using elemental powder blends based on titanium hydride powder and hydrogenated pre-alloyed Ti-6Al-4V powders with additions of ammonia carbonate as a removable space holder.
2. Porous Ti-6Al-4V alloys were characterized by uniform microstructure and acceptable content of impurities in material volume; however, the inner surface of pores was contaminated with increased content of oxygen and carbon remaining after the space holder removal process.
3. Contamination of the surface of the pores leads to embrittlement of the material samples, which is most pronounced during quasi-static compression. Under quasi-static and dynamic compression conditions, embrittlement is more pronounced for PA, in contrast to porous Ti64 obtained by the BEPM method. Therefore, the specific energy level absorbed in the case of PA materials is lower than that of porous titanium obtained by the BEPM method.

**Acknowledgements.** This work was co-financed by SPS NATO, grant number G5787 (Ukrainian team), and the Military University of Technology under research project UGB 22-742/2024 (Polish team).

## REFERENCES

[1] J.B. Manufacture, "Characterization and application of cellular metals and metal foams", *Prog. Mater Sci.,* vol. 46, pp. 559–632, 2001, doi:10.1016/S0079-6425(00)00002-5.

[2] D. Jafari, K.J.H.van Alphen, B.J. Geurts, W.W. Wits, L.C. Gonzalez, T.H.J. Vaneker, N. Ur Rahman, G.W. Römer , I. Gibson, "Porous materials additively manufactured at low energy: Single-layer manufacturing and characterization", *Mater. Des.,* vol. 191, pp. 108654, 2020, doi:10.1016/j.matdes.2020.108654.

[3] S.Y. Chena, C.N. Kuob, Y.L. Sud, J.C. Huanga, Y.C. Wua, Y.H. Lina, Y.C. Chunga, C.H. Ng, "Microstructure and fracture properties of open-cell porous Ti-6Al-4V with high porosity fabricated by electron beam melting", *Mater. Charact.,* vol. 138, pp. 255-262, 2018, doi:10.1016/j.matchar.2018.02.016.

[4] M. Kobashi, Sh. Miyake, N. Kanetake, "Hierarchical open cellular porous TiAl manufactured by space holder process", *Intermetallics,* vol. 42, pp. 32-34, 2013, doi:10.1016/j.intermet.2013.04.017

[5] B. Ye and D.C. Dunand, "Titanium foams produced by solid-state replication of NaCl powders", *Mater. Sci. Eng., A,* vol. 628, pp. 691-697, 2010, doi:10.1016/j.msea.2010.09.054.

[6] N. Takata, K. Uematsu, M. Kobashi, "Compressive properties of porous Ti–Al alloys fabricated by reaction synthesis using a space holder powder", *Mater. Sci. Eng., A,* vol. 697, pp. 66–70, 2017, doi:10.1016/j.msea.2017.05.015.

[7] A. Dmitruk, K. Naplocha, J. Pach, D. Pyka, G. Ziółkowski, M. Bocian, K. Jamroziak, "Experimental and Numerical Study of Ballistic Resistance of Composites Based on Sandwich Metallic Foams", *Appl. Compos. Mater.*, vol. 28, pp. 2011-2044, 2021, doi:10.1007/s10443-021-09957-0.

[8] S. Gaitanaros and S. Kyriakides, "On the effect of relative density on the crushing of open-cell foams under impact and energy absorption", *Int. J. Impact Eng.,* vol. 82, pp. 3e13, 2015, doi:10.1016/j.ijimpeng.2015.03.011.

[9] X.X. Zhang, H.W. Hou, L.S. Wei, Z.X. Chen, W.T. Wei, L. Geng, "High damping capacity in porous NiTi alloy with bimodal pore

architecture", *J. Alloys Compd.,* vol. 550, pp. 297–301, 2013, doi:10.1016/j.jallcom.2012.09.145.
[10] Y. Arakawa, M. Kobashi, N. Kanetake, "Foaming behavior of long-scale Al-Ti intermetallic foam by SHS mode combustion reaction", *Intermetallics,* vol. 41, pp. 22-27, 2013, doi:10.1016/j.intermet.2013.04.004
[11] A. Suzuki, N. Kosugi, N. Takata, M. Kobashi, "Microstructure and compressive properties of porous hybrid materials consisting of ductile Al/Ti and brittle Al3Ti phases fabricated by reaction sintering with space holder", *Mater. Sci. Eng., A,* vol. 776, no. 3, pp. 139000, 2020, doi:10.1016/j.msea.2020.139000 .
[12] P.E. Markovsky, J. Janiszewski, O.O. Stasyuk, D.G. Savvakin, D.V. Oryshych, P. Dziewit, "Mechanical energy absorption ability of titanium-based porous structures produced by various powder metallurgy approaches", *Materials,* vol. 16, pp. 3530, 2023, doi:0.3390/ma16093530.
[13] Y.G. Wang, J. Tao, J.L. Zhang, T. Wang, "Effects of addition of NH4HCO3 on pore characteristics and compressive properties of porous Ti-10%Mg composites", *Trans. Nonferrous Met. Soc. China,* vol. 21, no. 5, pp. 1074-1079, 2011, doi:10.1016/S1003-6326(11)60824-8.
[14] O.M. Ivasishin, V.M. Anokhin, A.N. Demidik, and D.G. Savvakin, "Cost-Effective Blended Elemental Powder Metallurgy of Titanium Alloys for Transportation Application", *Key Eng. Mater.,* vol. 188, pp. 55–62, 2000, doi:10.4028/www.scientific.net/KEM.188.55.
[15] O.M. Ivasishin and V.S. Moxson, "Low cost titanium hydride powder metallurgy", in: *Titanium Powder Metallurgy, Science, Technology and Applications,* Ma Qian, S.H. Froes Eds., Elsevier, 2015, ch. 8, pp.117-148, doi:10.3390/met10050682.
[16] J. Liu, S. He, H. Zhao, G. Li, M. Wang, "Experimental investigation on the dynamic behaviour of metal foam: from yield to densification", *Int. J. Impact Eng.,* vol. 114, pp. 69–77, 2018, doi:10.1016/j.ijimpeng.2017.12.016.
[17] Y. Duan, B. Du, X. Shi, B. Hou, Y. Li, "Quasi-static and dynamic compressive properties and deformation mechanisms of 3D printed polymeric cellular structures with kelvin cells", *Int. J. Impact Eng.,* vol. 132, pp.103303, 2019, doi:10.1016/j. ijimpeng.2019.05.017.
[18] B.T. Cao, B. Hou, H. Zhao, et al. "On the influence of the property gradient on the impact behavior of graded multilayer sandwich with corrugated cores". *Int. J. Impact Eng.*, vol. 113, pp. 98–105, 2018, doi:10.1016/j.ijimpeng.2017.11.017.
[19] G. Lutjering and J.C. Williams, *Titanium*, (2nd Edition) Springer, Berlin Heidelberg, New York. 438 P, 2007.
[20] D. Chen, S. Kitipornchai, J. Yang, "Dynamic response and energy absorption of functionally graded porous structures", *Mater. Des.,* vol. 140, no. 15. pp. 473-487, 2018, doi:10.1016/j.matdes.2017.12.019.
[21] Y. Qiao, D. Xu, S. Wang, Y. Ma, J. Chen, Y. Wang, H. Zhou, "Corrosion and Tensile Behaviors of Ti-4Al-2V-1Mo-1Fe and Ti-6Al-4V Titanium Alloys", *Metals,* vol. 9, no. 11, pp.1213, 2019, doi:10.3390/met9111213.
[22] B.G. Kutchko, A.G. Kim, "Fly ash characterization by SEM–EDS", *Fuel*, vol. 85, pp. 2537–2544, 2006, doi:10.1016/j.fuel.2006.05.016.
[23] X. Wang, J. Li, R. Hu, H. Kou, L. Zhou, "Mechanical properties of porous titanium with different distributions of pore size", *Trans. Nonferrous Met. Soc. Chine,* vol. 23, pp. 2317-2322, 2013, doi:10.1016/S1003-6326(13)62735-1.
[24] A. Aslan, B. Aksakal, F. Findik, "Fabrication of porous-Ti6Al4V alloy by using hot pressing technique and Mg space holder for hard-tissue biomedical applications", *J. Mater. Sci. Mater. Med.*, vol. 32, no. 80, 2021, doi:10.1007/s10856-021-06546-2.